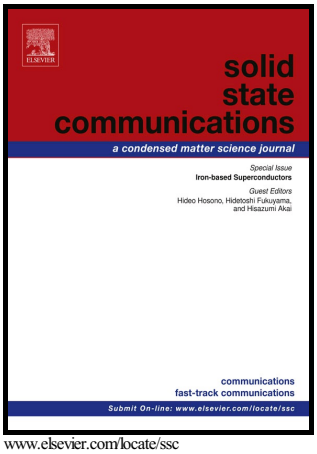

www.elsevier.com/locate/ssc

Vortex dynamics in phase separated $Tl_{0.58}Rb_{0.42}Fe_{1.72}Se_2$ crystals

N. Haberkorn, H. Troiani, A.M. Condó, Hangdong Wang, Qianhui Mao, Minghu Fang

PII: S0038-1098(16)30224-1
DOI: http://dx.doi.org/10.1016/j.ssc.2016.08.022
Reference: SSC13028

To appear in: *Solid State Communications*

Received date: 23 May 2016
Revised date: 23 August 2016
Accepted date: 31 August 2016

Cite this article as: N. Haberkorn, H. Troiani, A.M. Condó, Hangdong Wang, Qianhui Mao and Minghu Fang, Vortex dynamics in phase separated $Tl_{0.58}Rb_{0.42}Fe_{1.72}Se_2$ crystals, *Solid State Communications* http://dx.doi.org/10.1016/j.ssc.2016.08.022

Vortex dynamics in phase separated $Tl_{0.58}Rb_{0.42}Fe_{1.72}Se_2$ crystals

N. Haberkorn[1,2,*], H. Troiani[1,2], A. M. Condó[1,2], Hangdong Wang[3,4], Qianhui Mao[3], Minghu Fang[3,5]

[1] Consejo Nacional de Investigaciones Científicas y Técnicas, Centro Atómico Bariloche, Av. Bustillo 9500, 8400 San Carlos de Bariloche, Argentina.

[2] Instituto Balseiro, Bustillo 9500. S. C. de Bariloche. Argentina.

[3] Department of Physics, Zhejiang University, Hangzhou 310027,China.

[4] Department of Physics, Hangzhou Normal University, Hangzhou 310036, China.

[5] Collaborative Innovation Center of Advanced Microstructures, Nanjing 210093, China.

[*]Corresponding author. Tel : +54 0294 444 5147; fax: +54 0294 444 5299. nhaberk@cab.cnea.gov.ar

Abstract

We report the critical current density J_c and the vortex dynamics in phase-separated $Tl_{0.58}Rb_{0.42}Fe_{1.72}Se_2$ crystals by performing magnetization measurements. Structural investigation reveals micro- and nanoscopic phase separation between 122 (superconducting) and 245 (not superconducting) phases. Micrometric phase separation refers to 245 islands with typical diameters of 2 μm embedded in a multiply-connected 122 *superconducting network*. Nanoscopic phase separation refers to 245 nanoprecipitates embedded in the 122 superconducting paths. The 245 nanoprecipitates with size comparable to the coherence length produce strong vortex pinning. It was observed that the temperature dependence of the flux creep rate presents a peak at intermediate temperatures and magnetic fields lower than 0.5 T. The peak is systematically suppressed as the magnetic field is increased, and it could be related with relaxation generated by double-kink excitations. Double-kinks are low-energy depinning excitations usually associated with strong pinning produced by correlated disorder.

Keywords:

A. Superconductors; C. Structure and Characterization; D. Phenomena and Properties.

1. Introduction

The discovery of Fe-based superconductors (FeSCs) has renewed the interest in the phenomenology of type-II superconductors. The compounds share a layered structure, i. e., a square plane sheet of Fe^{2+}, tetrahedrally coordinated pnictogen (P, As) or chalcogen (S, Se, Te) anions [1]. Some of these materials, particularly iron selenide superconductors $A_{1-x}Fe_{2-y}Se_2$ (A = K, Rb, Cs, Tl) usually contain two distinct phases in their microstructure [2,3]: an insulating phase with the chemical formula $A_2Fe_4Se_5$ (related to the 245 phase), and a superconducting (SC) phase (related to the 122 phase) [4,5]. These structures result from Fe-deficiency and vacancy ordering [6]. The superconducting phase presents critical temperature (T_c) up to 32 K [7,8,9,10], and upper critical fields (H_{c2}) above 60 T [11]. The presence of inhomogeneities or phase coexistence in the nanoscale is well known for being beneficial for vortex line pinning [12,13,14]. Strong pinning and high critical current densities J_c are expected from precipitates with size comparable to the coherence length ξ [15]. Usually, artificially designed landscapes are built to study flux pinning mechanisms (strong and weak) in single FeSCs superconductors [13, 16, 17].

Vortex pinning arises from the interplay of several competing energies, namely the self-energy of the flux lines, the vortex-vortex interactions, the vortex inhomogeneity interactions and the thermal excitations [18]. Thermal fluctuations allow pinned vortices to oscillate around the potential energy minima, reducing the effective pinning energy due to thermal smearing. The vortices can also escape completely from the pinning centers through a variety of depinning excitations. Vortex motion still occurs for currents J lower than J_c at a much slower rate (due to thermally activated jumps out of the pinning centers) [19]. This flux creep mechanism implies a residual dissipation and is responsible for the time relaxation of persistent currents flowing in a superconducting closed loop. Depending on the temperature T and magnetic field H, the relaxation rate (S) is controlled by an activation energy that results from the interaction between the defects and the vortices. The theory of collective creep [20] (developed to explain vortex dynamics in cuprates) expresses the normalized relaxation rate $S(T,t) = -\frac{d(\ln J)}{d(\ln t)} = \frac{T}{U_0 + \mu T \ln(t/t_0)} = \frac{T}{U_0}\left(\frac{J}{J_c}\right)^{\mu}$ [eq. 1], where U_0 is the collective barrier in the absence of a driving force, t is the time, t_0 is an effective hopping attempt time and μ is the regime-

dependent glassy exponent. This approach successfully explains a wide range of vortex dynamics phenomena. The μ value is affected by the vortex-vortex and vortex-defects interactions. The expected values of μ for different depinning excitations (depending on field and on the pinning landscape) have been theoretically calculated [18]. The vortex physics in FeSCs has similitudes with that found in cuprates [15,21]. High flux creep rates and glassy relaxation have been reported [21]. From a technological point of view, the understanding of the different depinning mechanisms and their correlation with the superconducting parameters and the pinning landscape is essential, since electrical resistance derives from the dissipation associated with vortex motion.

In the first part of this article the microstructure of $Tl_{0.58}Rb_{0.42}Fe_{1.72}Se_2$ single crystals and the presence of nano- and microscopic phase separation are discussed. Next, the vortex dynamics which result from the strong pinning produced by 245 nanoprecipitates embedded in the 122 superconducting paths are examined. $Tl_{0.58}Rb_{0.42}Fe_{1.72}Se_2$ crystals present T_c = 32.5 K, $H_{c2}^{\|c-axis}\approx$ 60 T and upper critical field anisotropy γ = 2 [10, 11]. The results indicate that the J_c (*T*, *H*) dependences (i. e. extension of creep regimes and pinning mechanisms) are strongly affected by the phase coexistence between superconducting and non-superconducting regions. The analysis of temperature dependence of the flux creep rate *S* shows a peak at intermediate temperatures and fields up 0.5 T. This peak is gradually suppressed and it shifts to lower temperatures when the magnetic field is increased. These observations are consistent with those observed in $YBa_2Cu_3O_{7-\delta}$ (YBCO) single crystals with correlated defects [22] and the phenomenology could be associated with relaxation by double-kink excitations [23,24].

2. Experimental

Single crystals were grown using the Bridgman method. Detailed information is provided in reference [9]. First, Rb_2Se, Tl_2Se, Fe and Se powders (99.99%) were mixed in an appropriate stoichiometry and were placed in alumina crucibles and sealed in an evacuated silica tube. The mixture was heated up to 950 °C and held at this temperature for 6 hours. Then, the melted mixture was cooled down to 700 °C at a rate of 3 °C / h. Finally, the furnace was turned off and the mixture cooled down to room temperature. The crystals showed flat shiny surfaces and were easy to cleave. The composition of the crystals ($Tl_{0.58}Rb_{0.42}Fe_{1.72}Se_2$) was

determined by using an energy dispersive X-ray spectrometer (EDXS). Scanning electron microscopy (SEM) images were acquired with a FEI Nova Nano SEM230. The microstructure of the crystals was studied by transmission electron microscopy (TEM) with a Philips CM200UT microscope operating at 200kV. Specimens for TEM were prepared by grinding crystals in an agate mortar. X-ray diffraction (XRD) patterns were performed in a Panalytical Empyrean equipment.

The field, the temperature, and the time dependence of the persistent current density J_c (*H*, *T*, *t)* were obtained from the *irreversible* magnetization *M* (*H*, *T*, *t*) using the critical state model [25]. *M* (*H*, *T*, *t*) dependences were measured with a SQUID magnetometer in fields up to 5 T applied along the *c*-axis. The studied single crystal presents the following dimensions: thickness (*d*): 0.06 mm; width (*w*): 0.97 mm; and length (*l*): 2 mm. A similar vortex dynamics was observed in other crystals of the same batch. The flux creep rate, $S = -\frac{\delta(lnJ)}{\delta(lnt)}$, was recorded over periods of one hour. For longer periods (i.e. 2 hours) the *S* value did not exhibit significant modifications. The initial time was adjusted considering the best correlation factor in the log-log fitting of the J_c (*t*) dependence. The initial critical state for each creep measurement was generated by applying a field variation of $H \approx 4\ H^*$, where H^* is the field for full-flux penetration [26].

3. Results and discussion

Figure 1a shows the XRD pattern of a typical crystal used for this study. The XRD measurement was performed at room temperature and conditioned so as to observe (00*l*) reflections. Three sets of (00*l*) reflections were identified and similar XRD were obtained for other crystals of the same batch. This indicates the presence of, at least, three phases with *c* parameters: c_1 = 1.482 (0.001) nm, c_2 = 1.433 (0.002) nm and c_3 = 1.413 (0.002) nm. Usually, phase coexistence between an antiferromagnetic insulator phase (space group: *I*4/*m*) and a superconducting phase (space group: *I*4/*mmm*) is observed in $A_{1-x}Fe_{2-y}Se_2$ crystals [27]. The former could arise from superlattices with different lattice parameters from superstructures generated by different Fe vacancy order [2,3]. In addition, different insulator phases with different chemical composition and lattice parameters have been reported for $Rb_xFe_{2-y}Se_2$ [27], $(Tl,Rb)Fe_{2-y}Se_2$ [9] and $TlFe_xSe_2$ [10]. Figure 1b shows a SEM image of the

surface of a cleaved crystal. Two different types of patterns are observed: micrometric-size isolated islands (*i. e*. region A) with typical diameters of ≈ 2 μm and inhomogeneous interconnected networks (*i. e*. region B) with typical width of ≈ 2 μm. Similar features have been previously related to phase separation [3]. In order to obtain more detailed information of the microstructure, TEM images of the crystals were obtained. Figures 2*a*-*b* show typical TEM images corresponding to regions A and B indicated in Fig. 1*b*. Both images were obtained along the [00*l*] direction. Regions A, displayed in Fig. 2*a* (dark field TEM image), correspond to a superstructure generated by Fe-vacancy order [2, 3]. The superstructure spots observed in the reciprocal a*-b* plane can be characterized by a unique modulation wave vector q_1 =1/5[3a*+b*] (see inset Fig. 2*a*). Therefore, regions A correspond mainly to the non-superconducting 245 phase. Regions B, displayed in Fig. 2*b* (bright field TEM image), correspond to phase coexistence among the 245 and 122 phases (see inset Fig. 2*b*). The superconducting 122 phase presents a modulation with q_2 =1/2 [a*-b*] [2,3]. Nanoprecipitates embedded in the matrix can be identified (see arrows in Fig 2*b*). High resolution TEM images show that the precipitates present typical sizes of 5-10 nm. The distance between these nanoprecipitates varies from, approximately, 30 nm to 60 nm. Figure 2*c* shows a high resolution TEM image of a typical precipitate (approximate diameter: 11 nm) embedded in the matrix. The image was obtained along the [00*l*] direction. Fast Fourier transformations allow to identify q_2 (corresponding to the 122 phase) and q = -1/5[3a*+b*] (corresponding to the 245 phase) for the matrix and the precipitate, respectively. Figure 2*d* shows a region with phase coexistence between 122 and 245 phases. The fast Fourier transformations allow the identification of regions that can be associated with pure 122 and 245. In addition, spots corresponding to both phases appear in the fast Fourier transformation in regions where precipitates cannot be identified. This suggests that thin 122 / 245 layered structures along the *c*- axis are present [3,28]. In addition, distorted regions around precipitates are usually observed in TEM images. The described microstructure should affect significantly the vortex dynamics of the crystals. A large suppression of the superconducting volume is expected due to the substantial amount of 245 precipitates (regions A). The contribution of the regions A to vortex pinning could be practically disregarded (they are much larger than ξ_{ab} (0) ≈ 2.35 nm). The 245 nanoprecipitates embedded in the 122 slabs and local structural distortions at interfaces are expected to be the main sources of pinning in the superconducting paths. The

pinning can be either isotropic for nanoparticles or correlated for defects extended along the *c*-axis (such as amorphous areas or large angle grain boundaries). Layered 122 / 245 structures improve pinning when the field is parallel to the *a*-*b* plane [29].

The T_c in the crystals is 32.5 (0.1) K [11]. It is worth mentioning that the Meissner response obtained after zero field cool and **H** // c axis is consistent with the area of the crystal. Figure 3 shows J_c (H) at five different temperatures (T = 4.5 K, 10 K, 15 K, 20 K and 25 K). The J_c values were calculated from the Bean model. The resulting J_c (4.5 K, H = 0) was 15.5 kA cm^{-2}. The J_c values at all temperatures are affected by the reduction in the superconductor volume described above. Usually, larger J_c values are found in 122 systems with full superconductor volume [12,15,21]. For all temperatures, the J_c (H) dependences are weakly affected by self-field (SF) effects [30]. The SF estimated as $H^* = J_c * t$ is $\leq$ 100 Oe even at low temperatures, which is in agreement with the necessary magnetic field to invert the magnetization in the hysteresis loops (full flux penetration). In addition, none of the curves present a second peak in the magnetization or fishtail. The J_c (H) dependence at 4.5 K shows three clear regimes. Regime I (at low fields) shows a range of field where J_c (H) $\approx$ *constant* and it extends to $B^* \approx$ 0.12 T. This regime can be associated with a single vortex regime (SVR) with negligible vortex-vortex interaction [31]. The J_c (H) dependences obtained at temperatures above 4.5 K show that the regime is strongly suppressed by temperature. An apparent enhancement of B^* emerges at 25 K. Regime I is followed by Regime II at intermediate magnetic fields. At 4.5 K, the latter shows a power law dependence $J_c \propto H^{-\alpha}$ with α = 0.22. The value of α is usually related to the geometry of the pinning centers. The expected α value for strong pinning by nanoparticles is 0.55 [31]. In cuprates, when the vortices are pinned by correlated disorder or mixed pinning landscapes, it is strongly reduced from 0.55 to values as low as 0.2 [32]. For all temperatures above 4.5 K, regime II does not present a range of field where a power law regime can be clearly identified. Finally, at higher fields, regime III shows a more pronounced dependence in J_c (H). A criteria of α = 1 was used for the crossover between II and III (see arrows in Fig. 3) [31]. Regime III is usually associated with fast creep relaxation [21]. At T = 4.5 K regime III starts with $\mu_0 H \approx$ 1.6 T, which represents merely 3.5 % of the H_{c2} determined from electrical transport measurements [11]. This value is notoriously lower than those reported in other FeSCs with similar H_{c2} [33]. The crossover from II to III is usually influenced by the density of strong pinning centers and by dimensional effects [18].

Theoretically, a change should occur on the vortex dynamics for fields above the accommodation or matching field B_ϕ (the field at which the densities of defects and vortices are equal) [18]. For columnar defects, the dynamics of the vortices trapped between tracks is expected to be faster than for vortices trapped in the tracks, which reduces significantly the J_c values above B_ϕ. The second scenario is related to a change in the vortex dynamics produced by geometrical factors. As we mention above, the presence of phase coexistence in regions without precipitates suggests layered 122 / 245 structures along the *c*- axis [3]. A crossover in the flux creep from an elastic to a plastic regime is expected from the competence between the sample thickness (122 slabs) and the elasticity of the vortices [18]. Either two mechanisms (density of defects and layered structures), or a combination of both, could explain the low values of magnetic fields in the crossover from II to III of the J_c (H) dependences.

To understand the pinning mechanisms in the J_c (H, T) dependences, S (H, T) measurements were performed. Figure 4 shows S (T) at $\mu_0 H$ = 0.01 T, 0.05 T, 0.1 T, 0.3 T, 0.5 T, 0.75 T and 1 T. All the fields are above the estimated SF (< 0.01 T at low T) [30]. The most striking feature in the S (T) dependences is the presence of a peak for fields lower than 0.5 T. It was observed that, when the field is increased from 0.01 T to 0.5 T, the creep peak maximum shifts to lower temperatures and it disappears above 0.5 T. The peak is not manifest in S (T) dependences at larger magnetic fields (0.75 T and 1 T). A peak in the S (T) dependence was first observed in YBCO single crystals with columnar defects [34] and it was associated with relaxation by double kink excitations [23]. Double kinks are low energy excitations which produce fast relaxation from parallel or tilted columnar defects. This mechanism has been only observed in some materials such as cuprates with a source of correlated pinning (columnar rods, twin boundaries, dislocations or boundary between islands) [29,34,35,36]. The flux creep rates in materials that present double kinks exhibit several regimes. At low temperatures, thermal depinning occurs due to the formation of a critical nucleus which subsequently expands. Relaxation takes place via half-loops for fields below B_ϕ and when the size of the transverse nucleus is smaller than the distance between tracks. This mechanism presents a glassy exponent $\mu = 1$. When J decays and the deformation of the nucleus reaches the neighbor pin, the relevant excitations are double kinks, which transfer a vortex segment to a neighbor track [35]. A $\mu = 1/3$ has been theoretically predicted for this regime reaching a peak in S (T. For temperatures above this peak, the relaxation presents a plateau

corresponding to collective pinning. For fields above B_ϕ (all tracks are full), the double kink mechanism is suppressed and pinning becomes collective (the peak is not observed). The $B_\phi \approx$ 0.5 T corresponds to defects at typical distances of $\approx (\Phi_0 / B)^{1/2} \approx 65$ nm. This value is close to the distances between 245 nanoprecipitates observed in Fig. 2*b*, and it is considerably shorter than the 2 μm width of the superconducting networks. Another relevant feature in Fig. 4 is the fast increment in S (H) at low temperatures (T = 4.5 K), which indicates that the pinning is strongly reduced by magnetic field. This behavior could be ascribed to thin 122 / 245 layered structures along the *c*- axis, which overlap of the plastic and elastic relaxation mechanisms even at low magnetic fields. In addition, a fast increment in the S (T) dependences is observed for fields larger than B_ϕ = 0.5 T. The weak pinning for vortices exceeding $\mu_0 H$ = 0.5 T could be related to disorder in the 122 matrix (stressed interfaces and Fe vacancies). Random disorder should locally modify the superfluid density and increment vortex fluctuations [37].

Motivated by the source of the peak in $Tl_{0.58}Rb_{0.42}Fe_{1.72}Se_2$ crystals, we investigated the μ values at $\mu_0 H$ = 0.1 T. According to Maley analysis [38], the effective activation energy $U_{eff}(J)$ can be experimentally obtained considering that the current density decays as $\frac{dJ}{dt} = -\left(\frac{J_c}{\tau}\right) e^{-\frac{U_{eff}(J)}{T}}$. Thus, the final equation for the pinning energy is $U_{eff} = -T\left[ln\left|\frac{dJ}{dt}\right| - C\right]$ [eq. 2], where $C = ln(J_c/\tau)$ is a nominally constant factor. For an overall analysis, it is necessary to consider the function G (T), which results in $U_{eff}(J, T = 0) \approx U_{eff}\ (J,T)/G(T)$ [39]. Figure 5 shows the obtained Maley analyses for which, C = 14 and the G (T) dependence indicated in the inset, were used. In the limit of $J << J_c$ the μ exponent can be estimated as $\Delta \ln U(J) / \Delta \ln J$ [35]. The slopes below the maximum of the peak and at the plateau are 2 and 2.8, respectively. These values are larger than those previously observed in YBCO single crystals with columnar defects introduced by irradiation [34,35]. For instance, a value of μ = 2 has been reported for YBCO [40] single crystals with columnar defects at low fields and temperatures close to T_c. However, μ is usually affected by a combination of pinning centers (random point defects and nanoparticles) [32,34,36]. In $Tl_{0.58}Rb_{0.42}Fe_{1.72}Se_2$ the presence of a relaxation mechanism in agreement with double kinks, should be related to nanoprecipitates embedded in thin 122 superconducting slabs, or to defects originated by boundaries between phases assisting pinning produced by the 245 nanoprecipitates. For

example, in cuprates the twin boundaries assist pinning produced by nanoparticles [36]. As mentioned above, in TEM specimens for $Tl_{0.58}Rb_{0.42}Fe_{1.72}Se_2$,high distorted regions are usually observed around defects. Further research on these samples should be oriented to clarify the presence of correlated disorder by studying cross sectional TEM specimens. Focusing on vortex dynamics in crystals with more defined microstructures or artificial defects introduced by irradiation is necessary for a better understanding of these phenomena (peak in the relaxation and extension of the elastic regime) [34].

Figure 6 shows the *H-T* vortex phase diagram for the studied single crystal. The *S* peak position, the crossover to fast creep (obtained from the regime III) and a dashed line for the expected H_{c2} [11] are included. Both striking features, the peak and the extension of the elastic regimes, are associated with phase coexistence. The depinning temperature T_{dp}, which corresponds to vortices trapped in the tracks, is strongly affected by both, intrinsic thermal fluctuation and the diameter of the pinning centers [18, 23]. Its value can be estimated as $T_{dp} \approx T_c(\nu/(1+\nu))$, with $\nu = (r_d / 4\xi_{ab}(0)(1/\sqrt{Gi})$ (where $Tl_{0.58}Rb_{0.42}Fe_{1.72}Se_2$ has a Ginzburg number $Gi = \frac{1}{2}\left[\frac{\gamma T_c}{H_c^2(0)\xi^3(0)}\right]^2$ ~5x10^{-3}, being H_c the thermodynamic critical field and ξ_{ab} (0) = 2.35 nm [11]). In analogy with columnar defects and using $r_d \approx$ 2-5 nm as radio of the defects, $T_{dp} \approx$ 24 - 28 K is obtained. In YBCO, the peak corresponding to double-kink relaxation generally occurs between 20 and 40 K [34] and the T_{dp} for tracks with radio of 3 nm is above 70 K [32]. In $Tl_{0.58}Rb_{0.42}Fe_{1.72}Se_2$, the temperature for the maximum of the peak is reduced from ≈ 17 K to ≈ 10 K when the field is increased from 0.01 T to 0.5 T. This temperature corresponds to the same $J_c \approx$ 7.5 kA cm^{-2}. Considering weak temperature dependence of the parameters ξ, λ and γ, the peak by double kink excitations is expected to occur at the same (J_c/J_0) ratio [35]. On the other hand and as discussed above, the low fields for the crossover to regime III in J_c (*H*) (compared to H_{c2}), indicates that plastic vortex creep governs magnetic relaxation over a substantial part of the magnetic phase diagram. This fact could be attributed to weaker pinning of the vortices trapped between strong pinning centers in the superconducting slabs In addition, thin superconducting slabs are expected to affect the collective pinning regime due to a competence between their thickness and the elasticity of vortex lattice along the *c*-axis.

4. Summary

In summary, we have studied the vortex dynamics in $Tl_{0.58}Rb_{0.42}Fe_{1.72}Se_2$ crystals. The crystals present nano- and microscopic phase separation between 122 and 245 phases. The vortex phase diagram is strongly affected by the phase separation. The J_c (H) dependences are well described by strong pinning produced by 245 nanoprecipitates. The temperature dependence of the flux creep rates shows a peak for fields lower than 0.5 T. This peak shows similar features to those corresponding to relaxation by double-kink excitations in cuprates. In addition, the vortex dynamics changes significantly for fields above 0.5 T, which indicates weaker pinning for vortices trapped between the precipitates. Fast creep relaxation, usually associated with plastic creep, governs the vortex dynamics over a substantial part of the magnetic phase diagram.

Acknowledgements

We thank to D. Wilberger for technical assistance. The work in ZJU was supported by the National Basic Research Program of China (973 Program) under Grant Nos. 2015CB921004, 2012CB821404, and 2011CBA00103, the Nature Science Foundation of China (Grant Nos. 11374261, and 11204059) and Zhejiang Provincial Natural Science Foundation of China (Grant No. LQ12A04007), and the Fundamental Research Funds for the Central Universities of China. This work was partially supported by the ANPCYT (PICT 2015-2171). N H is member of the Instituto de Nanociencia y Nanotecnología (Argentina).

Figure 1. *a)* X-ray diffraction pattern for a $Tl_{0.58}Rb_{0.42}Fe_{1.72}Se_2$ crystal. *b)* SEM image of the *a*-*b* plane of a cleaved $Tl_{0.58}Rb_{0.42}Fe_{1.72}Se_2$ crystal. Regions A (islands) and B (stripe-like) indicate the two remarkable features in the surface topology of the crystals.

Figure 2. *a) b)* TEM images of regions A (dark field) and B (bright field) indicated in Fig. 1b. The insets correspond to the selected area electron diffraction (SAED) patterns obtained along the [00*l*] zone axis direction. *c)* High resolution TEM image of one of the precipitates

indicated with arrows in figure 2b. The insets correspond to fast Fourier transformations. Right corresponds to the matrix and left corresponds to the precipitate. *d*) Left: High resolution TEM image showing interpenetrated 122 and 245 phases. Right: Fast Fourier transformations of the indicated regions. The images were obtained along the [00*l*] zone axis direction.

Figure 3. Critical current density (J_c) vs. magnetic field (H) at different temperatures (4.5 K, 10 K, 15 K, 20 K and 25 K) obtained from irreversible magnetization hysteresis loops by using the Bean model.

Figure 4. Temperature dependence of the flux creep rate S at different magnetic fields (see panels). The measurements were divided in two panels for a clearer presentation. The values correspond to measurements obtained with **H** // *c*-axis.

Figure 5. Maley analysis at $\mu_0 H$ = 0.01 T for a $Tl_{0.58}Rb_{0.42}Fe_{1.72}Se_2$ crystals. Inset: Temperature dependence of the flux creep rate at $\mu_0 H$ = 0.01 T (right). G (T) function used for the Maley analysis (left).

Figure 6. Vortex-creep phase diagram for a $Tl_{0.58}Rb_{0.42}Fe_{1.72}Se_2$ crystals. The crossover for fast creep plastic was obtained from the crossover from the regime II to the regime III in Fig. 3. The H_{c2} (dashed line) was taken from [11]. The maximum of the relaxation peak for each temperature was obtained from Fig. 4.

References

[1] D. P. Chen and C. T. Lin, Supercond. Sci. Technol. **27** (2014) 103002 – 103002 (26).

[2] Z. Wang, Y. J. Song, H. L. Shi, Z. W. Wang, Z. Chen, H. F. Tian, G. F. Chen, J. G. Guo, H. X. Yang and J. Q Li, Phys. Rev B **83** (2011) 140505 – 140505 (4).

[3] Zhi-Wei Wang *et al*., J. Phys. Chem. C **116 (**2012) 17847-17852.

[4] Peiwen Gao *et al.*, Phys. Rev B **89** (2014) 094514-094514 (7).

[5] Zbigniew M. Stadnika, Pu Wang, Jan Żukrowski, Hang-Dong Wang, Chi-Heng Dong and Ming-Hu Fang, J. Alloys. Comp. **549** (2013) 288-294.

[6] Wei Li *et al*., 2012 Nature Physics **8** (2012) 126-130.

[7] J. G. Guo, S. F. Jin, G. Wang, S. C. Wang, K. X. Zhu, T. T. Zhou, M. He and X. L. Chen, Phys. Rev. B **82** (2010) 180520 - 180520 (4).

[8] A. Krzton-Maziopa, Z. Shermadini, E. Pomjakushina, V. Pomjakushin, M. Bendele, A. Amato, R. Khasanov, H. Luetkens and K. Conder, J. Phys.: Condens. Matter. **23** (2011) 052203 – 052203 (4).

[9] Hang-Dong Wang *et al*., EPL **93 (**2011) 47004 – 47004 (4).

[10] Minghu Fang, Hangdong Wang, Chiheng Dong, Zujuan Li, Chunmu Feng, Jian Chen, H. Q. Yuan, EPL **94** (2011) 27009 - 27009 (4).

[11] L. Jiao, Y. Kohama, J. L. Zhang, H. D. Wang, B. Maiorov, F. F. Balakirev, Y. Chen, L. N. Wang, T. Shang, M. H. Fang and H. Q. Yuan, Phys. Rev B **85** (2012) 064513 – 064513 (7).

[12] S. Demirdiş S, C. J. van der Beek, Y. Fasano, N. R. Cejas Bolecek, H. Pastoriza, D. Colson and F. Rullier-Albenque, Phys. Rev. B **84** (2011) 094517 – 094517 (8).

[13] K. J. Kihlstrom, L. Fang, Y. Jia, B. Shen, A. E. Koshelev, U. Welp, G. W. Crabtree, W. –K. Kwok, A. Kayani, S. F. Zhu and H. –H. Wen, Appl. Phys. Lett. **103** (2013) 202601-202601 (5).

[14] M. Miura, B. Maiorov, T. Kato, T. Shimode, K. Wada, S. Adachi and K. Tanabe, Nat. Commun. **4** (2013) 2499-2506.

[15] C. J. van der Beek *et al.,* Phys. Rev. B **81** (2010) 174517 – 174517 (11).

[16] Y Nakayima et al. Phys. Rev B 80 (2009) 012510- 012510 (4).

[17] T. Tamegai et al. Supercond. Scie Tech. **25** (2012) 084008-084008 (14).

[18] G. Blatter, M. V. Feigelman, V. B. Geshkenbein, A. I. Larkin and V. M. Vinokur, Rev. Mod. Phys. **66 (**1994) 1125-1388.

[19] M. Tinkham, 2004 Introduction to Superconductivity 2nd edn (New York: Dover).

[20] M. V. Feigel'man, V. B. Geshkenbein, A. I. Larkin and V. M. Vinokur, Phys. Rev. Lett. **63** (1989) 2301-2304; M. V. Feigel'man, V. B. Geshkenbein and V. M. Vinokur, Phys. Rev. B **43** (1991) 6263-6265.

[21] R. Prozorov *et al*., Phys. Rev. B **78** (2008) 224506 – 224506 (9).

[22] L. Civale, A. D. Marwick, T. K. Worthington, M. A. Kirk, J. R. Thompson, L. Krusin-Elbaum, Y. Sun, J. R. Clem and F. Holtzberg, Phys. Rev. Lett. **67** (1991) 648-651.

[23] L. Krusin-Elbaum *et al*., Phys. Rev. B **53 (**1996) 11744-11750.

[24] D. R. Nelson and V. M. Vinokur, Phys. Rev. Lett. **68** (1992) 2398-2401; Phys. Rev. B **48** (1993) 13060 -13097.

[25] A. M. Campbell and J. E. Evetts, Adv. Phys. **21** (1972) 199 - 428.

[26] Y. Yeshurun, A. P. Malozemoff, A. Shaulov, Rev. Mod. Phys. **68** (1996) 911 - 949.

[27] Yoshiaki Kobayashi,Shohei Kototani, Kazuki Ohishi, Masayuki Itoh, Akinori Hoshikawa, Toru Ishigaki, and Masatoshi Sato. J. Phys. Soc. Jpn. **84** (2015) 044710-044710 (7).

[28] Y. J. Yan *et al.* Scientific Reports 2 (2012) 212- 212 (5).

[29] S. R. Foltyn, L. Civale, J. L. MacManus-Driscoll, Q. X. Jia, B. Maiorov, H. Wang and M. Maley, Nat. Mat **6** (2007) 631-642.

[30] N. Haberkorn *et. al.*, Phys. Rev. B **84** (2011) 94522- 94522 (7).

[31] C. J. van der Beek, M. Konczykowski, A. Abal'oshev, I. Abal'osheva, P. Gierlowski, S. J. Lewandowski, M. V. Indenbom and S. Barbanera, Phys. Rev. B **66** (2002) 024523 – 024523 (10).

[32] N. Haberkorn *et al.*, Phys. Rev. B **85** (2012) 174504 – 174504 (7).

[33] N. Haberkorn, B. Maiorov, I. O. Usov, M. Weigand, W. Hirata, S. Miyasaka, S. Tajima, N. Chikumoto, K. Tanabe, L. Civale, Phys. Rev B **85 (**2012) 014522- 014522 (7).

[34] L. Civale, Supercond. Sci. Technol. **10** (1997) A11-A28.

[35] J. R. Thompson, L. Krusin-Elbaum, L. Civale, G. Blatter and C. Field, Phys. Rev Lett. **78** (1997) 3181-3184.

[36] M. Miura *et al.* Phys. Rev B **83** (2011) 184519- 184519 (8).

[37] Jeehoon Kim *et al.* Phys. Rev B **86** (2012) 144509 -144509 (6).

[38] M. P. Maley, J. O. Willis, H. Lessure and M. E. McHenry, Phys. Rev. B **42 (**1990) 2639 - 2642.

[39] J. G. Ossandon, J. R. Thompson, D. K. Christen, B. C. Sales, Y. Sun and K. W. Lay Phys. Rev. B **46 (**1992) 3050 - 3058.

[40] M. Konczykowski Physica C **209 (**1993) 247-250.

Highlights

- Transmission electron microscopy analysis reveals phase coexistence.
- Vortex dynamics for $Tl_{0.58}Rb_{0.42}Fe_{1.72}Se_2$ single crystals is reported.
- Flux creep rates present a peak at intermediate temperatures for fields smaller than 0.5 T